Article

JOURNAL OF COMPOSITE MATERIALS

Journal of Composite Materials
2022, Vol. 56(12) 1879–1889

DOI: 10.1177/00219983221084407
journals.sagepub.com/home/jcm
SAGE

Electrical properties of melt-mixed polypropylene and as-grown carbon nanofiber composites: Analysis of their interphase *via* the AC conductivity modeling

Antonio J Paleo[1], Najoia Aribou[2], Yassine Nioua[2], Zineb Samir[2], Lisete Fernandes[3], J Agostinho Moreira[4] and Mohammed E. Achour[2]

Abstract

The morphology, crystallinity, and electrical conductivity (σ' and σ'') as a function of frequency of polypropylene (PP) melt-extruded with different amounts of as-grown carbon nanofibers (CNFs) from 0 to 1.4 vol. % are examined. The PP/CNF composites present CNF aggregates randomly distributed within the PP and an insulator–conductor transition at CNF contents near 0.9 vol. %. The degree of crystallinity of PP/CNF composites with loadings of 1.4 vol. % increases ~15% with respect to the neat PP (~34%), with $\sigma' \sim 8.6 \times 10^{-5}$ S m^{-1} ($\sigma'' \sim 8.3 \times 10^{-4}$ S m^{-1}) at 2 MHz. In addition, the values of the electrical conductivity σ_{int}' ~2.9×10^{-6} S m^{-1} (σ_{int}''~3.7×10^{-4} S m^{-1}) at 2 MHz, as a result of the interphase (ϕ_{int} ~0.05 vol. %) of the 1.4 vol. % PP/CNF composites, are estimated by the use of a modified generalized effective medium model (GEM). The analysis gathered in here indicates that the interphase between the polymer and the conducting particle may have a quantifiable effect on the electrical properties of carbon-based polymer composites, and this fact should not be neglected in the production of conducting polymer composites (CPCs) with enhanced electrical properties.

Keywords

carbon nanofibers, polypropylene, interphase, polymer composites, generalized effective medium model

Introduction

The investigation of insulating polymers filled with carbonaceous conductive materials such as carbon black (CB),[1] carbon nanotubes (CNTs),[2] graphene derivatives,[3] etc., have attracted much attention due to their numerous applications, which include from sensors,[4] energy harvesting,[5] energy storage[6] to high DC voltage cables[7] and electromagnetic radiation shielding, and interference (EMI) materials.[8] Among carbonaceous conductive particles, vapor-grown carbon nanofibers (CNFs), produced by chemical vapor deposition (CVD) of catalyst nanoparticles under a mixture of gaseous hydrocarbons, are an interesting choice due to their high aspect ratio combined with low density, chemical and thermal stability, and ease of production in large quantities, which significantly reduce their costs.[9] This type of carbon structures have shown diameters in the range of 50–200 nm, hollow cores of 30–90 nm, and lengths of 50–100 μm.[10] It is well known by the percolation theory that the conducting polymer composites (CPCs) display a sudden jump in the electrical conductivity (σ) as the content of carbon fillers exceeds a certain critical value, known as the electrical percolation threshold (ϕ_c).[11] Thus, the dependence of σ on the content of the carbon filler (ϕ) is expressed as $\sigma \alpha (\phi - \phi_c)^t$ for $\phi > \phi_c$, where t is a critical exponent, which is assumed to be universal, and it depends on the dimensionality

[1]2C2T, Centro de Ciência e Tecnologia Têxtil, Universidade Do Minho, Portugal
[2]Faculty of Sciences, Laboratory of Material Physics and Subatomic, Ibn Tofail University, Morocco
[3]UME, Electron Microscopy Unit and CQVR, Centre of Chemistry-Vila Real, Trás-os-Montes and Alto Douro University, Portugal
[4]IFIMUP -Institute of Physics for Advanced Materials, Faculdade de Ciências da Universidade Do Porto, Portugal

Corresponding authors:
Antonio J Paleo, Universidade Do Minho, Campus Azurem, Guimarães 4800-058, Portugal.
Email: ajpaleovieito@2c2t.uminho.pt

ME Achour, LASTID Laboratory, Department of Physics, Faculty of Sciences, University Ibn Tofail, BP 133, 14000 Kenitra, Morocco.
Email: me.achour@uit.ac.ma

of the system.[12] Despite this simplified model estimates quite well the σ of CPCs based on carbon nanostructures,[2] the accurate analysis of the electrical conductivity in such type of polymer composites is not completely achieved yet.[13] For instance, the above approach does not take also into account some important particularities such as the processing method, the carbon filler shape, the polymer–filler interaction, and the resistance contact between carbon fillers, which cause that the exponent t is not universal as expected by that model.[14] Accordingly, other models have been proposed to explain the electrical properties of conducting composite materials such as the models based on the effective medium theories (EMT).[15] However, the models derived by the EMT often fail when, for instance, the CPCs achieve high values of σ.[16] Thus, several attempts such as the generalized effective medium model (GEM) developed by McLachlan, which is a direct combination of the EMT with the percolation theory, were proposed to overcome some of the above-described shortcomings.[17] Moreover, despite the good agreement with experimental data, the physical parameters provided by the GEM normally results also dependent on the particular type of CPCs analyzed.[18] It is in this context that we have undertaken this study, which complements a former study focused on the dielectric spectroscopy analysis at room temperature of melt-extruded polypropylene (PP) with as-grown CNFs by the universal power laws (UPLs).[19] In the present work, the AC electrical conductivity at room temperature of the same type of PP/CNF composites is used to test the validity of the GEM model. Moreover, the potential of a modified GEM[20] that takes into consideration the effect of the interphase between the CNFs and the PP is also examined. It is observed that the modified GEM presents a good agreement with the experimental measurements, from which the values of the volume concentration and complex electrical conductivity corresponding to the interphase of the PP/CNF composites could be estimated over the range of frequency analyzed.

Experimental details

Materials

The constituent materials were polypropylene (Borealis EE002AE) and PR 25 AG carbon nanofibers in the form of powder (Applied Sciences, Inc.). The CNFs, grown catalytically from gaseous hydrocarbons using metallic catalyst particles,[21] were used as received without any further chemical modification. They are characterized by presenting a structure composed of a graphitic tubular core surrounded by a stacked-cup inner layer followed by a pyrolytic hydrocarbon outer layer.[22] It is noted that this particular CNF grade is synthesized in as-grown condition without the utilization of any postprocessing method. Morphologically, the CNFs show hollow core diameters in the range of 30–90 nm, total diameters of 100–200 nm, and lengths of 30–100 μm,[22,23] with conductivities of 10^3 S m^{-1}.[23]

Processing method

The PP/CNF composites with six CNF volume concentrations from pristine melt-extruded PP to 1.4 vol. % were prepared on a modular laboratory-scale intermeshing mini, co-rotating twin-screw extruder, with a screw diameter of 13 mm, barrel length of 31 cm, and an approximate L/D ratio of 26, coupled to a cylindrical rod dye of approximately 2.85 mm of diameter. A detailed description of the melt extrusion conditions has been previously published.[24] After extrusion, the PP/CNF composites were compression-molded into specimens with the appropriate geometries for the specific characterization. In particular, squared films of dimensions 10 × 10 mm^2 and thickness of 0.5 mm with Au electrodes deposited on both sides by thermal evaporation were used for the AC electrical testing.

Characterization

An Olympus BH2 transmittance light microscope was used to observe first the microstructure of the PP/CNF composites. The analyzed samples were cut into rectangles of 4 × 2 mm and 10 μm in thickness using a sliding Leitz 1300 microtome equipped with a glass slicing knife. The samples were placed between the microscope glass slide and a cover glass. Canada balsam glue (Alfa Aesar, CAS#8007–47-4) was used to prevent curling up or corrugating. All samples were cured under convenient pressure prior to analysis. The morphological characterization and the CNF dispersion within the PP were examined in high vacuum mode ($<10^{-5}$ mbar) by using a FEI Quanta 400 W scanning electron microscope (SEM) at an accelerating voltage of 30 kV with an extra 25–30° tilt. The cross sections of the composites were cryo-fractured in liquid nitrogen. The surfaces were sputter-coated with 3 nm of gold prior to the analysis. The X-ray diffraction (XRD) data were collected at room temperature by a PANalytical X'Pert Pro diffractometer, equipped with X'Celerator detector and secondary monochromator in θ/2θ Bragg-Brentano geometry. The measurements were carried out using a Cu–Kα radiation ($\lambda\alpha_1$ =1.54,060 Å and $\lambda\alpha_2$ = 1.54,443 Å) 40 kV and 30 mA, at a resolution of 0.017° per step, with a 100-s integration per step, over the range 2θ=10–60°. Differential scanning calorimetry (DSC) tests were performed using a Mettler–Toledo DSC822 instrument (Giessen, Germany) in a nitrogen atmosphere. In the nonisothermal experiments, the specimens were heated from 25°C to 190°C at a rate of 10°C min^{-1} to eliminate any previous thermal history and then cooled down to 25°C at a rate of 10°C min^{-1}. Following this, the samples were heated to 190°C at the same rate of 10°C min^{-1}.

The direct current conductivity σ_{DC} at room temperature was performed using an experimental setup composed by a picoammeter Keitheley model 6487 and a digital control DC power supply TENMA model 72–10,495 as described in a previous work[19]. The capacitance (C) and dielectric losses tan δ (w) at room temperature were measured by using a Quadtech 1929 LCR precision meter at frequencies (f) between 430 Hz and 2 MHz, with an applied signal of 0.5 V. The real $\varepsilon'(w)$ and the imaginary $\varepsilon''(w)$ parts of the complex dielectric permittivity ε(w) were calculated by the equations

$$\acute{\varepsilon}(w) = C(w)\frac{d}{\varepsilon_0 S}. \quad (1)$$

$$\acute{\varepsilon}(w) = \acute{\varepsilon}(w)\tan\delta(w). \quad (2)$$

The parameters d and S are the thickness and the surface area of the squared films, respectively, $w = 2\pi f$ is the angular frequency, and ε_0 is the permittivity of vacuum (8.85×10^{-12} F m^{-1}). In turn, the complex conductivity $\sigma(\omega) = \sigma'(\omega) + i\sigma''(\omega)$ was obtained by using the following expressions

$$\acute{\sigma}(w) = w\ \varepsilon_0\acute{\varepsilon}(w). \quad (3)$$

$$\acute{\sigma}(w) = w\ \varepsilon_0\acute{\varepsilon}(w). \quad (4)$$

Results and discussions

Morphologic, X-ray diffraction and Differential scanning calorimetry analysis

The micrographs corresponding to the transmittance light microscope of the PP/CNF composites with 0.2, 0.5, 0.9, and 1.4 vol. % of CNFs are illustrated in Figure 1. The emergence of agglomerate results is evident from the first lowest CNF loadings of 0.2 and 0.5 vol. % (Figures 1(a) and (b)), though the biggest aggregate with a length of more than 50 μm is observed for samples with CNF loadings of 0.9 vol. % (Figure 1(c)). Interestingly, the presence of higher number of agglomerates in the sample with the highest content of CNFs 1.4 vol. % (Figure 1(d)) could promote the formation of the necessary paths for electric conduction.

The representative SEM micrographs at different magnifications of the PP/CNF composites with 1.4 vol. % of CNFs (Figure 2) show how the individual CNFs are distributed within the aggregates. It is reminded that the as-received PR 25 AG grade used is not treated with any debulking method after its production. This is important to note because the debulking post-treatment allows requiring much less energy for the CNF dispersion in the melted polymer,[24] and consequently, it makes more difficult their processing by melt extrusion. Therefore, only PP/CNF composites with CNF loadings up to 1.4 vol. % were produced under the processing conditions presented in this work. Thus, it is expected that the PR 25 AG grade provides low levels of dispersion and low electrical conductivity values, even for the PP/CNF composites with the highest loading of CNFs (1.4 vol. %). In addition, Figure 2(b) clearly shows how the CNFs protruded far from the polypropylene, which is a signal of poor wetting.

The XRD patterns of the neat extruded PP samples and PP with 0.4, 0.9, and 1.4 vol. % CNF loadings are shown in Figure 3. The extruded PP showed a single-phase α with peaks at approximately 14.2° (110), 17.0° (040), 18.6° (130), 21.3° (111), and 22.0° (041),[25] whereas the other two lower peaks at ~ 25.6° and 28.9° are assigned to the (060) and (220) planes of the same phase α, respectively.[26] On the other hand, the PP/CNF composites did not show significant differences with respect to the XRD pattern of PP, which indicates that the PP/CNF composites do not promote the presence of different polypropylene phases. Likewise, the XRD peak located at about 22° has also been associated with the diffraction line of the CNFs.[26] Moreover, other works have related the peaks at ~ 25.6° (060) with the hexagonal crystal structure of the graphite in CNTs.[27]

The DSC analyses shown in Figure 4(a) were performed to obtain further information about the influence of CNFs on the crystallization behavior of PP, which is expected to affect the electrical properties of the PP/CNF composites. In particular, the melting temperature (T_m) and degree of crystallinity (ΔX_c) in % of PP and PP/CNF composites corresponding to the second heating scans are shown in Figure 4(b), where the ΔX_c of the neat melt-extruded PP and PP/CNF composites was calculated by

$$\Delta X_C = \frac{\Delta H_M}{\Delta H_0 f_{PP}} \times 100\ \%. \quad (5)$$

ΔH_m is the sample melting enthalpy and $\Delta H_0 f_{PP}$ is the melting enthalpy of the 100% crystalline PP (207 J g^{-1}).[28] The PP showed a single melting peak at ~ 166°C in accordance with other works that report melt-compounding PP-based composites ,[23] whereas a slight decrease in the melting temperature is noticed for the PP/CNF composites in Figure 4(b). Notably, the results in Figure 4(b) show a clear increase of ΔX_c ~ 15% with respect to the PP (~34%) for PP/CNF composites with 1.4 vol. %. The latter result has been associated to the degree of stretching rise of the macromolecular polymer chains caused by the loading with the nanoparticles.[23]

AC conductivity analysis by the universal power laws

The DC electrical conductivities at room temperature of the PP/CNF composites as a function of CNF concentration are represented in Figure 5. A clear increase is observed for PP/CNF composites with loadings of 1.4 vol. % (~8×10^{-6} S

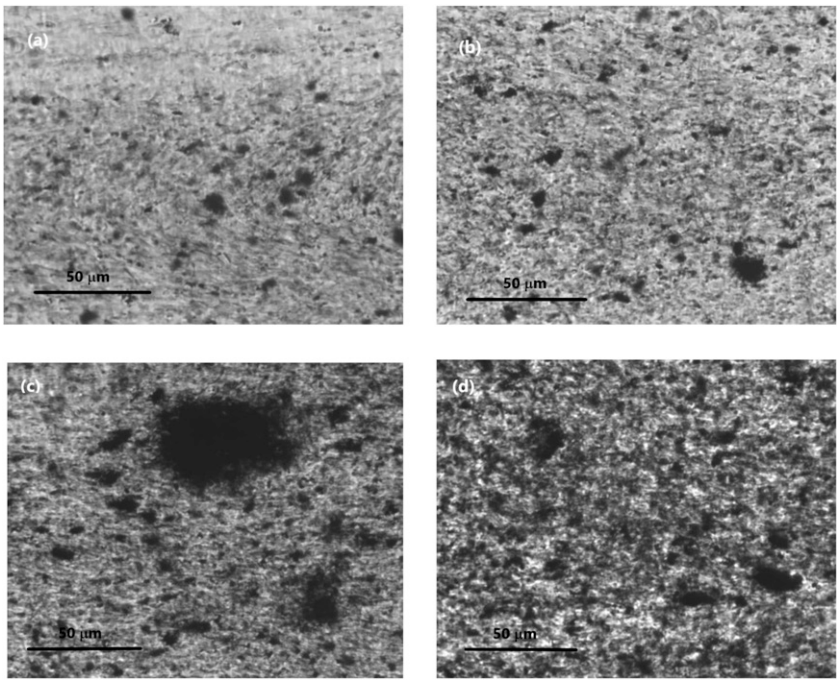

Figure 1. Optical transmission micrographs of PP/CNF composites with 0.2 vol. % (a), 0.5 vol. % (b), 0.9 vol. % (c), and 1.4 vol. % (d) of CNFs.

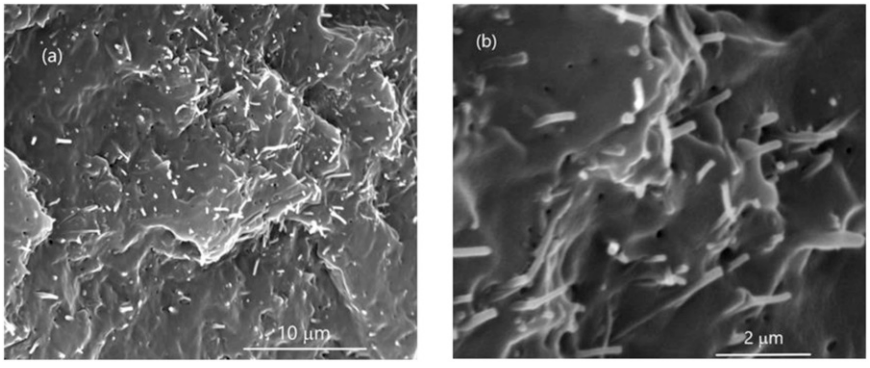

Figure 2. Representative SEM micrographs of PP/CNF composites with 1.4 vol. % of CNFs at different magnifications 10 μm (a) and 2 μm (b).

m^{-1}). According to the percolation theory, the σ_{DC} can be expressed by the power law relationship $(\phi - \phi_c)^t$, which relates the experimental σ_{DC} with the filler concentration ϕ, where ϕ_c is the percolation threshold and t is the critical exponent associated with the dimensional character of the network.[11,12] Although Figure 5 evidences an insulator–conductor transition between 0.9 and 1.4 vol. %, the values of σ_{DC} could not be fitted by that power law because the impossibility of producing PP/CNF composites with higher CNF contents under the processing conditions presented in this work.

A comparison table with the σ_{DC} of this work (8×10^{-6} S m^{-1}) at CNF loadings of 1.4 vol. % (equivalent to 3 wt. %) and reported literature for PP/CNF composites based on CNFs produced by Applied Sciences, Inc., are summarized in Table 1 to provide some context on the levels of σ_{DC} achieved in similar PP/CNF composites. The table includes the CNF type, processing method, CNF content, and corresponding σ_{DC} to that CNF content. Notably, it is found a broad dispersion of σ_{DC}, from the lowest values of 1×10^{-7} S m^{-1} reported for melt-mixed PP/CNF with 15 wt. % of CNFs[29] to the highest values of 17.8 S m^{-1} achieved in melt-extruded PP/CNF with 9 vol. % of CNFs[30].

The electric responses of polymer composites containing conductive fillers can be accurately described by the universal

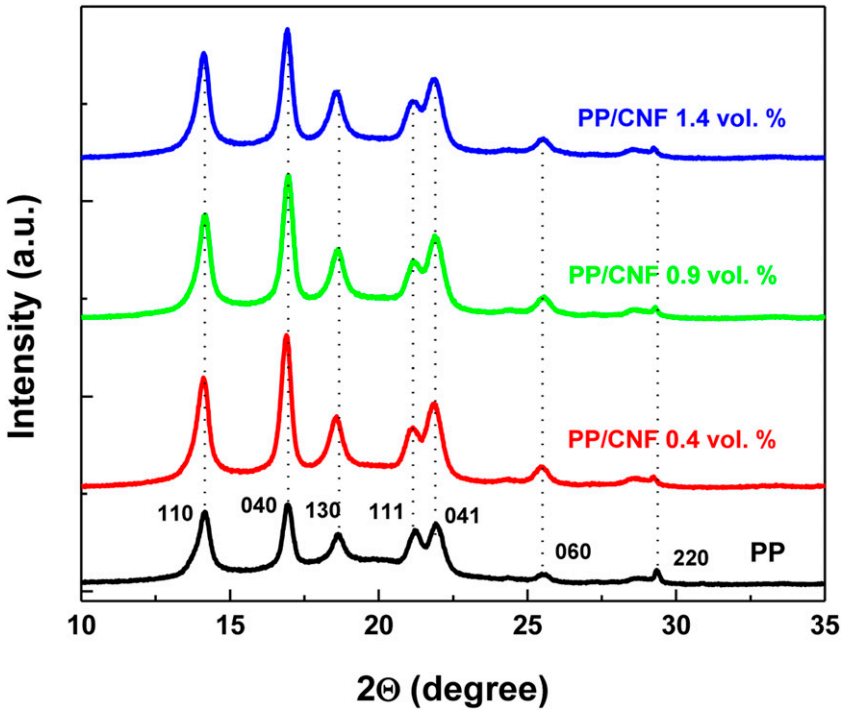

Figure 3. XRD patterns and assignment of the most important lines due to the phase α of PP and PP/CNF composites. Dotted lines are guides for the eyes.

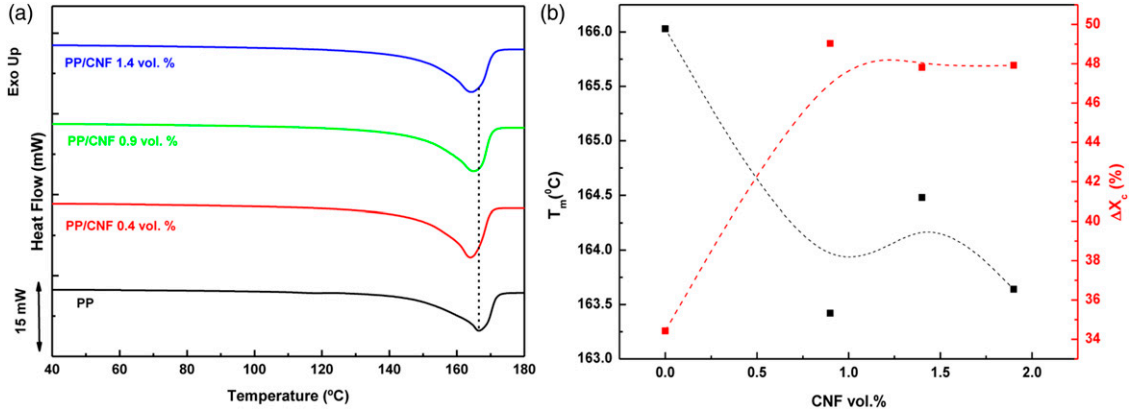

Figure 4. DSC thermographs (a) and T_m and ΔX_c (b) of PP and PP/CNF composites. Dotted lines are guides for the eyes.

power laws (UPLs), which were experimentally and theoretically obtained by Jonscher[35,36] and Dissado and Hill[37,38]

$$\sigma'(\omega) \propto \omega^{n1}, \tag{6}$$

$$\sigma''(\omega) - \sigma''\infty \propto \omega^{n2} \tag{7}$$

where σ''_∞ is the high-frequency imaginary part of the electrical conductivity. It must be noted that the dielectric relaxation is governed by three processes according to Dissado and Hill. The fastest of them, called as the flip transition, arises from configurational tunneling. In short, the *n1* and *n2* exponents are a measure of the correlation between individual flip transitions. If *n1(or n2)=0,* a flip can occur without correlation to neighboring dipoles, whereas if *n1 (or n2)=1,* this transition is fully correlated.[39] The experimental variations of $\sigma'(\omega)$ and $\sigma''(\omega)$ at room temperature in the range from 430 to 2×10^6 Hz are represented in Figure 6. In general, $\sigma'(\omega)$ increases with increasing CNF concentration for the whole range of frequencies. Moreover, the $\sigma'(\omega)$ of the pure PP and PP/CNF composites with up to 0.9 vol. % CNFs increases almost linearly with frequency, demonstrating their nearly insulating

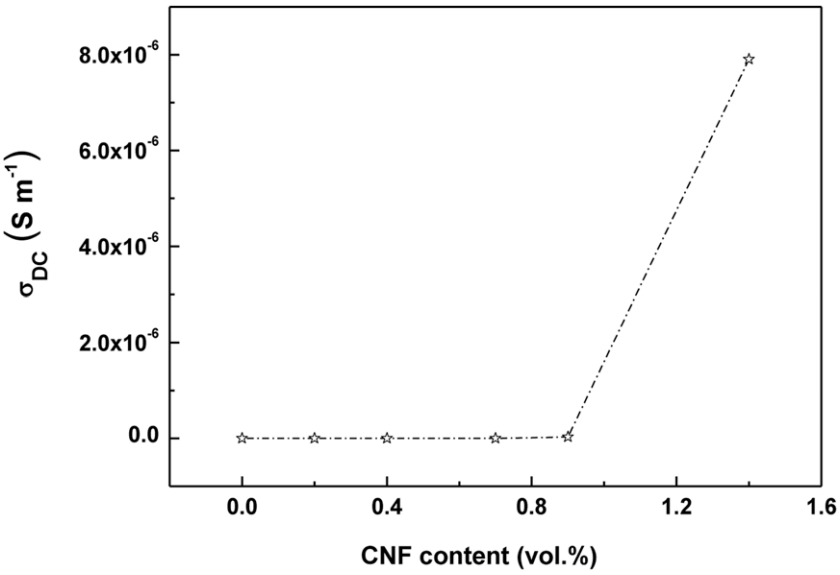

Figure 5. DC electrical conductivity as a function of CNF contents in PP/CNF composites (the dash-dot lines are to guide the eyes).

Table 1. σDC values of PP/CNF composites based on CNFs of Applied Sciences, Inc. The term * means that the CNF used is Pyrograph® III, but authors do not specify the exact grade.

CNF type	Method	Content	σ_{DC} (S m^{-1})	Reference
PR 24 AG (treated)	Melt mixing	10 wt. %	2×10^{-1}	23
PR 19 HT	Melt extrusion	9 vol. %	17.8	30
PR 24 PS XT	Melt mixing	10 wt. %	1×10^{-2}	31
Pyrograph® III*	Melt mixing	15 wt. %	1×10^{-7}	29
PR 24 LHT XT	Solvent dispersion	5 wt. %	2.1×10^{-4}	32
Pyrograph® III*	Melt extrusion	5 wt. %	1×10^{-6}	33
PR 24 HHT XT	Melt mixing	6 wt. %	4.5×10^{-5}	34
PR 25 AG	Melt extrusion	1.4 vol. %	8×10^{-6}	This work

behavior. However, the $\sigma'(\omega)$ of PP/CNF composites with 1.4 vol. % of CNFs, shown in Figure 6(a), is almost constant up to a critical frequency *fc* (~20 kHz). This frequency-independent characteristic indicates that these PP/CNF composites achieve an insulating–conducting transition near 0.9 vol. % of CNFs.[40] The $\sigma''(\omega)$, in turn, shows always a frequency-dependent behavior for all the PP/CNF composites. Notably, a slight jump between 0.7 and 0.9 vol. % is observed in $\sigma''(\omega)$, which can be associated to the formation of some conducting CNF paths in PP/CNF 0.9 vol. % composites. In addition, $\sigma''(\omega)$ increases with the higher amount of CNFs at each frequency. This is related to the high number of charge carriers injected by the higher CNF contents.[41] The $\sigma'(\omega)$ and $\sigma''(\omega)$ are fitted by equations (6) and (7) in order to extract the exponents *n1* and *n2*, which are reported in Table 2 together with σ''_{∞}. (The fitting was made above the frequency of the maximum loss (5.8×10^5 rad s^{-1}) in the case of PP/CNF 1.4 vol. % composites). Table 2 shows how the average values of exponent *n* decreases from ~1.0 (for PP) to 0.65 (for PP/CNF 1.4 vol. %), which means that the PP/CNF composites are becoming more conductive with the raise of CNF vol. % contents. Likewise, as the amount of CNFs increases, the σ''_{∞} decreases. The latter result can be attributed to the enhanced dielectric properties caused by the interfacial polarization between the CNF aggregates and the PP .[19]

AC conductivity analysis by the generalized effective medium model

The generalized effective medium model (GEM) is used to examine the complex conductivity of the PP/CNF composites as a function of the CNF content.[42,43] The PP/CNF composites are assumed as binary and homogenous systems, where the electrical contact between the PP and CNFs is considered negligible, and the CNFs are supposed to be in contact with each other. In particular, the GEM can be expressed by the "two-exponent phenomenological percolation equation" (TEPPE)[2,44,45]

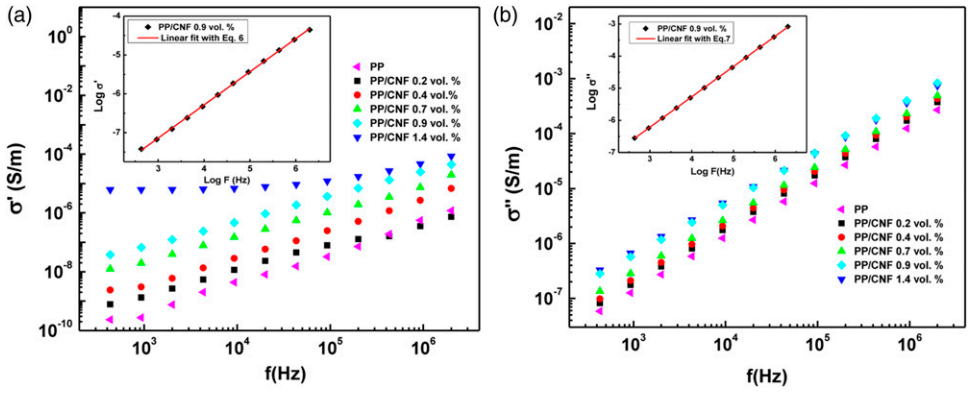

Figure 6. AC complex conductivity $\sigma'(\omega)$ (a) and $\sigma''(\omega)$ (b) versus frequency of PP and PP/CNF composites. The red solid lines in the inset figures are the least-square linear fits to UPL equations (6) and (7) of 0.9 vol. % PP/CNF composites.

Table 2. Exponents *n*1, *n*2, and σ''_∞ of PP/CNF composites extracted from UPL equations (6) and (7).

Sample	n1	n2	n (average)	σ''_∞ (S m^{-1})
PP	1.03 ± 0.06	1.00 ± 0.04	1.01 ± 0.02	1.09 ± 0.11 x 10^{-9}
PP/CNF 0.2 vol. %	0.81 ± 0.09	0.98 ± 0.03	0.90 ± 0.02	1.22 ± 0.13 x 10^{-9}
PP/CNF 0.4 vol. %	0.96 ± 0.06	0.96 ± 0.05	0.96 ± 0.02	1.77 ± 0.01 x 10^{-8}
PP/CNF 0.7 vol. %	0.86 ± 0.08	0.92 ± 0.06	0.89 ± 0.02	2.00 ± 0.02 x 10^{-8}
PP/CNF 0.9 vol. %	0.85 ± 0.09	0.84 ± 0.06	0.85 ± 0.12	7.93 ± 0.17 x 10^{-8}
PP/CNF 1.4 vol. %	0.58 ± 0.10	0.72 ± 0.10	0.65 ± 0.01	3.21 ± 0.01 x 10^{-7}

$$(1-\phi)\frac{\left(\sigma_m^{1/s}-\sigma^{1/s}\right)}{\left(\sigma_m^{1/s}+A\sigma^{1/s}\right)}+\phi\frac{\left(\sigma_f^{1/t}-\sigma^{1/t}\right)}{\left(\sigma_f^{1/t}+A\sigma^{1/t}\right)}=0, \quad (8)$$

where σ_f, σ_m, and σ are the complex conductivity of the CNFs, the PP, and the PP/CNF composites, respectively; ϕ is the volume concentration of the CNFs; and A is a constant described in terms of the percolation threshold by $A=\frac{1-\phi_c}{\phi_c}$. The s and t exponents of equation (8) describe the behavior of the complex conductivity below and above ϕ_c, respectively. In this analysis, the electrical conductivities considered for the PP and CNFs were $\sim 10^{-10}$ and 10^3 S·m^{-1}, respectively, and an estimated ϕ_c=0.89 vol. % was used based on the previous results (Figure 7). Following the aforementioned reasoning, the equations (9) and (10) are deduced from equation (8), where s and t are adjustable parameters calculated from the fitting of the experimental data

$$For\ \sigma_f \to \infty\ \sigma=\sigma_m\left(\frac{\phi_c}{\phi_c-\phi}\right)^s \phi \le \phi_c. \quad (9)$$

$$For\ \sigma_m \to 0\ \sigma=\sigma_f\left(\frac{\phi-\phi_c}{1-\phi_c}\right)^t \phi \ge \phi_c. \quad (10)$$

Accordingly, the σ' and σ'' at 2 MHz of PP/CNF composites as a function of the CNF vol. % are plotted in Figure 7(a) and Figure 7(b), respectively. The dashed blue lines correspond to the best fit with the TEPPE equation, when the universal values $t \sim 2$ and $s \sim 0.7$ of the percolation theory for 3D networks are used, whereas the dashed green lines correspond to the best fit of the TEPPE equation, when t and s are considered adjustable parameters. Figure 7(a) shows that the σ' extracted by the TEPPE equation is only valid for CNF contents below the threshold (0.89 vol. %). Moreover, this discrepancy is even worst for the case of σ'', as it is shown in Figure 7(b), where the TEPPE equation is not valid for CNF amounts above 0.2 vol. %. On the contrary, a good agreement is found in σ' (w) and σ'' (w), when the t and s exponents are considered adjustable and dependent on frequency (dashed green lines of Figure 7(b)). It must be noted that the values of s ($0.79 \le s \le 1$) and t ($2.9 \le t \le 3.6$) as a function of frequency obtained for PP/CNF composites shown in Table 3 diverge from the universal values $s \sim 0.87$ and $t \sim 2$ provided by the TEPPE equation for 3D networks.[46] In this respect, nonuniversal t exponents ranging from 1 to 6.27[47,48] and s exponents ranging from 0.37 to 1.28[45] have been reported in 3D percolative systems. This deviation of s and t can be caused by the fact that the GEM does not take into account important parameters, such as the particle geometry,[49] existence of aggregates,[50] and interphase region between the CNFs and PP matrix,[51] which should play an important role in the final properties of the

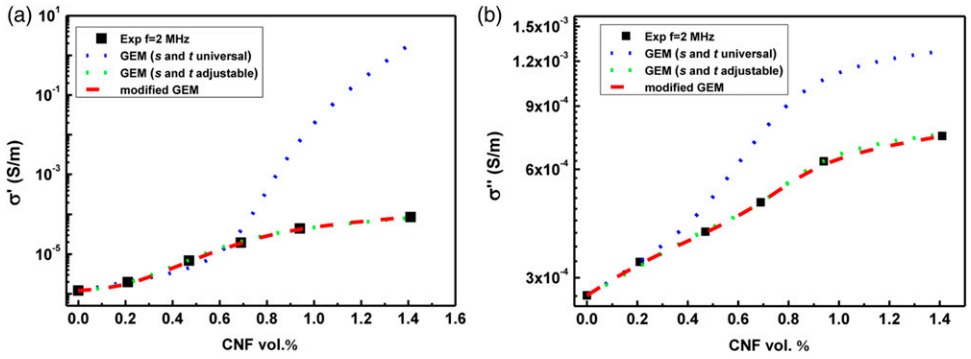

Figure 7. Experimental (full symbols) and fittings (dashed line curves) by the GEM and modified GEM of σ' (a) and σ'' (b) at 2 MHz in PP/CNF composites.

Table 3. Adjustable *s* and *t* exponents obtained by TEPPE equation and *k*, σ_{int}', and σ_{int}'' obtained by the modified GEM at different frequencies of PP/CNF composites.

f (kHz)	s	t	k	$\sigma'_{int}(S\,m^{-1})$	$\sigma''_{int}(S\,m^{-1})$
9.3	0.79±0.1	2.9±0.1	0.20±0.04	1.13±0.08×10^{-8}	2.75±0.10×10^{-6}
20	0.79±0.1	3.0±0.06	0.15±0.03	7.56±0.09×10^{-8}	4.09±0.11×10^{-6}
43	0.81±0.07	3.0±0.06	0.13±0.03	9.55±0.09×10^{-8}	9.18±0.12×10^{-6}
92	0.82±0.07	3.1±0.03	0.11±0.02	1.32±0.093×10^{-7}	1.71±0.13×10^{-5}
200	0.93±0.06	3.3±0.03	0.09±0.02	5.98±0.09×10^{-7}	3.86±0.15×10^{-5}
400	0.96±0.1	3.3±0.03	0.08±0.02	8.12±0.092×10^{-7}	5.69±0.13×10^{-5}
900	0.97±0.1	3.4±0.06	0.07±0.01	1.01±0.09×10^{-6}	1.34±0.09×10^{-4}
2000	1.0±0.1	3.6±0.1	0.04±0.01	2.86±0.09×10^{-6}	3.73±0.08×10^{-4}

PP/CNF composites. Therefore, a modified GEM, which includes the volume fraction (ϕ_{int}) and the complex conductivity of the interphase (σ_{int}), is proposed in this study[20]

$$\sum \phi_{int} \frac{\left(\sigma_{int}^{1/t} - \sigma^{1/t}\right)}{\left(\sigma_{int}^{1/t} + A\sigma^{1/t}\right)} = 0 \tag{11}$$

which it simplifies to

$$(1-\phi-\phi_{int})\frac{\left(\sigma_m^{1/t} - \sigma^{1/t}\right)}{\left(\sigma_m^{1/t} + A\sigma^{1/t}\right)} + \phi_{int}\frac{\left(\sigma_{int}^{1/t} - \sigma^{1/t}\right)}{\left(\sigma_{int}^{1/t} + A\sigma^{1/t}\right)} + \phi\frac{\left(\sigma_f^{1/t} - \sigma^{1/t}\right)}{\left(\sigma_f^{1/t} + A\sigma^{1/t}\right)} = 0 \tag{12}$$

where ϕ_{int} depends strongly on the filler concentration ϕ and on the critical parameter *k* given by Todd and Vo[52,53] as

$$\phi_{int} = k\phi\frac{1-\phi}{1+k\phi}. \tag{13}$$

Consequently, the σ' and σ'' at 2 MHz provided by the modified GEM of the PP/CNF composites as a function of the CNF vol. % are represented as dashed red lines in Figure 7(a) and Figure 7(b), respectively. Specifically, the results were obtained by solving numerically the equation (12) through an interactive procedure, where *k*, σ_{int}', and σ_{int}'' are adjustable parameters and the universal value $t \sim 2$ is used. Figures 7(a) and (b) show clearly that the modified GEM fits correctly with the experimental data. In particular, the best fit for PP/CNF composites at 2 MHz is obtained for $\sigma_{int}' = 2.86 \pm 0.09 \times 10^{-6}$ S·m^{-1}, $\sigma_{int}'' = 3.73 \pm 0.08 \times 10^{-4}$ S·m^{-1}, and $k = 0.04 \pm 0.01$. Similarly, the *k*, σ_{int}', and σ_{int}'' for the PP/CNF composites at the rest of frequencies are presented in Table 3. As it can be seen there, the increase of frequency causes the decrease of the critical parameter k, which means that the effect of the interphase becomes weaker as the frequency raises. On the contrary, an increase of the σ_{int}' and σ_{int}'' with the higher frequency values is observed, which is consistent with the increment of σ' and σ'' with frequency presented in Figure 6.

Figure 8 represents the variation of ϕ_{int} of PP/CNF composites as a function of the CNF volume fraction calculated by the equation (13) at different frequencies. It is worth noting that ϕ_{int} increases linearly with the increment of the CNF volume fraction for all the frequencies. This is an expectable result since the large amount of CNFs should cause an increase of the interphase area between the CNFs

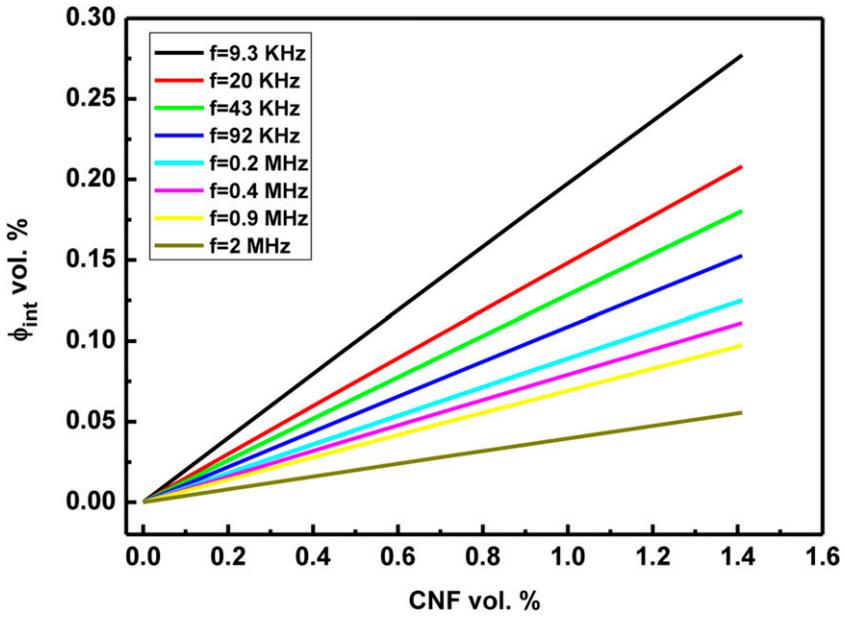

Figure 8. Interphase vol. % as a function of CNF vol. % at different frequencies in PP/CNF composites.

and the polypropylene. About this, a previous work has proposed the existence of an interphase composed by two layers on melt-mixed PP/CNF composites produced with a similar type of CNFs (PR 24 AG). That work estimates that the outer layer of that interphase must have a thickness of 10^2 nm comparable to the radius of gyration of the polymer, whereas the inner layer must have a thickness of the order of 10° nm.[51] Moreover, similarly to k, the increase of frequency causes the decrease of ϕ_{int}, which evidences that the interphase contribution to the complex conductivity becomes lower as the frequency increases.[54] In this regard, comparable behaviors of ϕ_{int} and k with frequency, calculated by this modified GEM, were reported for carbon black–loaded epoxy composites.[20]

Conclusions

The AC electrical conductivity of melt-extruded low-conducting polypropylene composites with different volume concentrations of CNFs from 0 to 1.4 vol. % at room temperature is reported. The morphologic and structural properties showed that the CNFs formed aggregates randomly distributed within the PP, whereas the degree of crystallinity of the PP was increased in the PP/CNF composites. An insulating–conducting transition was detected near 0.9 vol. % of CNFs. As expected, the highest loaded PP/CNF composites (1.4 vol. %) showed the highest conductivities ($\sigma' \sim 8.6 \times 10^{-5}$ and $\sigma'' \sim 8.3 \times 10^{-4}$ S m^{-1}) at 2 MHz with respect to the PP ($\sigma' \sim 1.2 \times 10^{-6}$ and $\sigma'' \sim 2.7 \times 10^{-4}$ S m^{-1}). In addition, the AC electrical conductivity was systematically analyzed by the universal power laws (UPLs), the generalized effective medium model (GEM), and a modified GEM, which takes into consideration the effect of the interphase between the CNFs and the PP. The GEM showed limited applicability for CNF contents above 0.9 vol. %, whereas the values of σ' (w) and σ''(w) were fitted accurately by the modified GEM, from which the interphase (in vol. %) and conductivity corresponding to that interphase of the PP/CNF composites could be extracted. This study indicates that the interphase between the polymer and the conducting particles may have a quantifiable effect on the electrical properties of carbon-based polymer composites, and this fact should not be neglected in the production of CPCs with the desired electrical properties.

ORCID iDs

A. J. Paleo https://orcid.org/0000-0002-4688-5794
M. E. Achour https://orcid.org/0000-0002-7786-0645

Declaration of conflicting interests

The author(s) declared no potential conflicts of interest with respect to the research, authorship, and/or publication of this article.

Funding

This study was funded by FCT-Foundation for Science and Technology: "Plurianual" 2020–2023 Project UIDB/00264/2020.

References

1. Achour ME, Brosseau C and Carmona F. Dielectric relaxation in carbon black-epoxy composite materials. *J Appl Phys* 2008; 103.
2. McLachlan DS, Chiteme C, Park C, et al. AC and DC percolative conductivity of single wall carbon nanotube polymer composites. *J Polym Sci B: Polym Phys* 2005; 43: 3273–3287.

3. Yang L, Weng W, Fei X, et al. Revealing the interrelation between hydrogen bonds and interfaces in graphene/PVA composites towards highly electrical conductivity. *Chem Eng J* 2020; 383: 123126.
4. Zhou C-G, Sun W-J, Jia L-C, et al. Highly Stretchable and Sensitive Strain Sensor with Porous Segregated Conductive Network. *ACS Appl Mater Inter* 2019; 11: 37094–37102.
5. Kröning K, Krause B, Pötschke P, et al. Nanocomposites with p- and n-Type Conductivity Controlled by Type and Content of Nanotubes in Thermosets for Thermoelectric Applications. *Nanomaterials (Basel, Switzerland)* 2020; 10: 1–15.
6. Ameli A, Wang S, Kazemi Y, et al. A facile method to increase the charge storage capability of polymer nanocomposites. *Nano Energy* 2015; 15: 54–65.
7. Azizi S, David E, Fréchette MF, et al. Electrical and thermal phenomena in low-density polyethylene/carbon black composites near the percolation threshold. *J Appl Polym Sci* 2019: 136.
8. Bhadra S, Rahaman M and Noorunnisa Khanam P. Electrical and electronic application of polymer-carbon composites. In: Rahaman M, Khastgir D and Aldalbahi AK (eds) *Carbon-containing polymer composites*. Singapore: Springer; 2019, pp. 397–455.
9. Al-Saleh MH and Sundararaj U. A review of vapor grown carbon nanofiber/polymer conductive composites. *Carbon* 2009; 47: 2–22.
10. Yang S, Benitez R, Fuentes A, et al. Dielectric analysis of VGCNF reinforced polyethylene composites. *Composites Sci Technology* 2007; 67: 1159–1166.
11. Nigro B, Grimaldi C and Ryser P. Tunneling and percolation transport regimes in segregated composites. *Phys Review. E, Stat Nonlinear, Soft Matter Physics* 2012; 85: 011137.
12. Stauffer D and Aharony A. *Introduction To Percolation Theory*: Second Edition. 2018.
13. Dang Z-M, Yuan J-K, Zha J-W, et al. Fundamentals, processes and applications of high-permittivity polymer-matrix composites. *Prog Mater Sci* 2012; 57: 660–723.
14. Silva J, Cardoso P, Paleo AJ, et al. On the origin of the electrical response of vapor grown carbon nanofiber + epoxy composites. *E-polymers* 2012; 12(1).
15. Lagarkov AN, Sarychev AK, Smychkovich YR, et al. Effective medium theory for microwave dielectric constant and magnetic permeability of conducting stick composites. *J Electromagn Waves Appl* 1992; 6: 1159–1176.
16. El Malhi M, Achour ME, Lahjomri F, et al. Dielectric response in carbon black-epoxy resin composites. *J Mater Sci Lett* 1999; 18: 613–616.
17. Zakaria MY, Sulong AB, Sahari J, et al. Effect of the addition of milled carbon fiber as a secondary filler on the electrical conductivity of graphite/epoxy composites for electrical conductive material. *Composites B: Eng* 2015; 83: 75–80.
18. Elhad Kassim SA, Achour ME, Costa LC, et al. Prediction of the DC electrical conductivity of carbon black filled polymer composites. *Polym Bull* 2015; 72: 2561–2571.
19. Paleo AJ, Samir Z, Aribou N, et al. Dielectric spectroscopy of melt-extruded polypropylene and as-grown carbon nanofiber composites. *Eur Phys J E* 2021: 44.
20. Aribou N, Nioua Y, Bouknaitir I, et al. Prediction of filler/matrix interphase effects on AC and DC electrical properties of carbon reinforced polymer composites. *Polym Composites* 2019; 40: 346–352.
21. Tibbetts GG, Doll GL, Gorkiewicz DW, et al. Physical properties of vapor-grown carbon fibers. *Carbon* 1993; 31: 1039–1047.
22. Lawrence JG, Berhan LM and Nadarajah A. Structural transformation of vapor grown carbon nanofibers studied by HRTEM. *J Nanoparticle Res* 2008; 10: 1155–1167.
23. Aldica GV, Ciurea ML, Chipara DM, et al. Isotactic polypropylene–vapor grown carbon nanofibers composites: Electrical properties. *J Appl Polym Sci* 2017: 134.
24. Paleo AJ, Sencadas V, Van Hattum FWJ, et al. Carbon nanofiber type and content dependence of the physical properties of carbon nanofiber reinforced polypropylene composites. *Polym Eng Sci* 2014; 54: 117–128.
25. Zheng W, Lu X, Ling Toh C, et al. Effects of clay on polymorphism of polypropylene in polypropylene/clay nanocomposites. *J Polym Sci Part B: Polym Phys* 2004; 42: 1810–1816.
26. Chipara M, Hamilton J, Chipara AC, et al. Fourier transform infrared spectroscopy and wide-angle X-ray scattering: Investigations on polypropylene-vapor-grown carbon nanofiber composites. *J Appl Polym Sci* 2012; 125: 353–360.
27. Ganß M, Satapathy BK, Thunga M, et al. Structural interpretations of deformation and fracture behavior of polypropylene/multi-walled carbon nanotube composites. *Acta Materialia* 2008; 56: 2247–2261.
28. Yuan Q and Misra RDK. Impact fracture behavior of clay-reinforced polypropylene nanocomposites. *Polymer* 2006; 47: 4421–4433.
29. Lozano K, Bonilla-Rios J and Barrera EV. A study on nanofiber-reinforced thermoplastic composites (II): Investigation of the mixing rheology and conduction properties. *J Appl Polym Sci* 2001; 80: 1162–1172.
30. Kuriger RJ, Alam MK, Anderson DP, et al. Processing and characterization of aligned vapor grown carbon fiber reinforced polypropylene. *Composites A: Appl Sci Manufacturing* 2002; 33: 53–62.
31. Lee S-H, Hahn J-R, Ku B-C, et al. Effect of carbon nanofiber structure on crystallization kinetics of polypropylene/carbon nanofiber composites. *Bull Korean Chem Soc* 2011; 32: 2369–2376.
32. Li Y, Zhu J, Wei S, et al. Poly(propylene) nanocomposites containing various carbon nanostructures. *Macromolecular Chem Phys* 2011; 212: 2429–2438.
33. Sui G, Jana S, Zhong WH, et al. Dielectric properties and conductivity of carbon nanofiber/semi-crystalline polymer composites. *Acta Materialia* 2008; 56: 2381–2388.

34. Muñoz-Ávila JM, Sánchez-Valdes S, Yáñez-Flores I, et al. Influence of carbon nanofiber functionalization and compatibilizer on the physical properties of carbon nanofiber reinforced polypropylene nanocomposites. *Polym Composites* 2018; 39: 3575–3585.
35. Jonscher AK. The measurement and interpretation of dielectric properties. *Thin Solid Films* 1983; 100: 329–334.
36. Jonscher AK. The universal dielectric response and its physical significance. *IEEE Trans Electr Insul* 1992; 27: 407–423.
37. Dissado LA and Hill RM. Anomalous low-frequency dispersion. Near direct current conductivity in disordered low-dimensional materials. *J Chem Soc Faraday Trans 2* 1984; 80: 291–319.
38. Dissado LA and Hill RM. The fractal nature of the cluster model dielectric response functions. *J Appl Phys* 1989; 66: 2511–2524.
39. Forsman H, Andersson P and Bäckström G. Dielectric relaxation of glycerol and n-propyl alcohol at high pressure. *J Chem Soc Faraday Trans 2* 1986; 82: 857–868.
40. He L-X and Tjong S-C. Alternating current electrical conductivity of high-density polyethylene-carbon nanofiber composites. *The Eur Phys J E* 2010; 32: 249–254.
41. Barnoss S, Aribou N, Nioua Y, et al. *Dielectric Properties of PMMA/PPy Composite Materials*. Dordrecht: Springer, 2020, pp. 259–271.
42. McLachlan DS. Analytical functions for the dc and ac conductivity of conductor-insulator composites. *J Electroceramics* 2000; 5: 93–110.
43. McLachlan DS. A quantitative analysis of the volume fraction dependence of the resistivity of cermets using a general effective media equation. *J Applied Physics* 1990; 68: 195–199.
44. McLachlan DS, Blaszkiewicz M and Newnham RE. Electrical Resistivity of Composites. *J Am Ceram Soc* 1990; 73: 2187–2203.
45. McLachlan DS and Sauti G. The AC and DC conductivity of nanocomposites. *J Nanomater* 2007: 2007.
46. McLachlan DS. The percolation exponents for electrical and thermal conductivities and the permittivity and permeability of binary composites. *Physica B: Condensed Matter* 2021; 606.
47. Lee S-I, Song Y, Noh TW, et al. Experimental observation of nonuniversal behavior of the conductivity exponent for three-dimensional continuum percolation systems. *Phys Rev B* 1986; 34: 6719–6724.
48. Chiteme C and McLachlan D. AC and DC conductivity, magnetoresistance, and scaling in cellular percolation systems. *Phys Rev B* 2003; 67: 024206.
49. Prinkey MT, Lakhtakia A and Shanker B. On the Extended Maxwell-Garnett and the Extended Burggeman approaches for dielectric-in-dielectric composites. *Optik (Jena)* 1994; 96: 25–30.
50. Gong S, Zhu ZH, Li J, et al. Modeling and characterization of carbon nanotube agglomeration effect on electrical conductivity of carbon nanotube polymer composites. *J Appl Phys* 2014: 116.
51. Chipara M, Lozano K, Hernandez A, et al. TGA analysis of polypropylene-carbon nanofibers composites. *Polym Degrad Stab* 2008; 93: 871–876.
52. Vo HT, Todd M, Shi FG, et al. Towards model-based engineering of underfill materials: CTE modeling. *Microelectronics J* 2001; 32: 331–338.
53. Todd MG and Shi FG. Characterizing the interphase dielectric constant of polymer composite materials: Effect of chemical coupling agents. *J Appl Phys* 2003; 94: 4551–4557.
54. Liu X, Wu Y, Wang X, et al. Effect of interphase on effective permittivity of composites. *J Phys D: Appl Phys* 2011: 44.